Journal of
Materials Chemistry C

Sensitization of near-infrared LnIII [Ln = Yb or Nd] ions using water-soluble, band gap tuneable 3-MPA-capped CdS nanoparticles

SCHOLARONE™
Manuscripts

Journal Name

ARTICLE

Sensitization of near-infrared Ln^III [Ln = Yb or Nd] ions using water-soluble, band gap tuneable 3-MPA-capped CdS nanoparticles

A. de Bettencourt-Dias,[*] R.A. Tigaa

We synthesized 3 – 4 nm crystalline, cubic phase, monodisperse 3-mercaptopropionato capped CdS nanoparticles (3-MPA-NPs) with different heating reaction times. Their aqueous fluorescence emission quantum yields were in the range 2.0 – 3.4%, and biexponential lifetimes, in the range 34 – 50 ns (surface states) and 303 – 477 ns (core states) which increased linearly with increasing heating reaction time. The NPs were then decorated with near-infrared emitting Nd^III and Yb^III ions through chelation to the surface carboxylato groups of 3-mercaptopropionato (3-MPA-Ln-NPs). Excitation of these NPs at their maximum absorption wavelength resulted in emission of the surface-bound Ln^III ions with efficiencies in the range 0.01 – 0.02%. The overlap of the excitation spectra of the Ln^III-containing systems 3-MPA-Ln-NPs with the absorption spectra of the NPs indicates that energy was transferred from the NPs to the metal ions coordinated to the surface 3-MPA.

Introduction

The optical properties of trivalent lanthanide (Ln^III) ions make them uniquely suited for imaging and sensing applications.[1-3] The emission spectra have narrow bands (FWHM = 10 nm) arising from the core nature of the $4f$ electrons, as these are shielded from the ligand field by the filled $5s$ and $5p$ orbitals.[3-5] The emissive excited states are long-lived, with lifetimes in the μs to ms range, due to the Laporte forbidden f-f transitions.[4] As a result of the forbidden nature of the f-f transitions, Ln^III ions have low molar absorptivities ($\varepsilon = 1$ M^{-1} cm^{-1}), and their direct excitation is inefficient.[4] Therefore, efficient sensitization of Ln^III ion emissions is achieved, for example, through organic ligands capable of transferring energy from excited singlet (^1S) and triplet (^3T) levels to the emissive f excited state.[3-5] While there is ongoing interest in new organic ligands as sensitizers, the syntheses often require elaborate procedures and tedious purification steps.[6-9]

Alternatively, nanoparticles (NPs) can be used as optical antennae to sensitize the Ln^III-centred emission. The size-dependent band gap tuneable properties of NPs and the ease of synthesis provide a facile route to new platforms for the sensitization.[10-14] For instance, host-lattices such as CdS, CdSe, ZnS, In_2O_3, LaF_3, YVO_4, $NaYF_4$, Y_2O_3, $ZnAl_2O_4$ and $ZnGa_2O_4$ doped with Ln^III ions have been shown to transfer energy to the emissive f levels following excitation of the host-lattice at a wavelength of absorption.[10, 15-26] The doping of Ln^III ions into these host-lattices reduces the quenching of the metal-centred

luminescence by high energy oscillators such C-H, O-H and N-H vibrations from solvent molecules.[15] Efforts to enhance the sensitization efficiency of Ln^III ions has led to the synthesis of Ln^III-doped NPs that are surface functionalized with organic ligands with ^3T energy levels better matched with the f emissive energy levels of the metal ions.[16, 26-28] Chowdhury and co-workers[27] demonstrated that enhancement of Ln^III-centred luminescence can be achieved by functionalizing the surface of the NPs with ligands capable of chelating and sensitizing Ln^III ions.[29, 30] Imbert, Mazzanti and co-workers[30] reported the sensitization of visible and near-infrared (NIR) Ln^III ions by InPZnS@ZnSe/ZnS NPs grafted with Ln^III-complexes. We demonstrated that easily synthesized and isolated ZnS NPs capped with thiol-appended 2,6-pyridine-derivatives[29] and equally easily accessible surface functionalized carbon NPs[31] were not only able to chelate Eu^III and Tb^III ions, but also sensitized their emission following excitation of the NPs. With the ZnS NPs work, we showed that there is direct energy transfer from the NP to visible emitting Ln^III ions using the non-chromophore 3-mercaptopropionato (3-MPA) as surface capping ligand; the ligand is not directly involved in the sensitization of the metal ions.[29] Despite the Ln^III-centred emission, the energy transfer from the ZnS NPs to visible emitting Eu^III and Tb^III ions was inefficient, which was attributed to the mismatch of the wide band gap (bulk ZnS = 3.7 eV or 29,840 cm^{-1}) of the ZnS NPs relative to the emissive f levels of the Eu^III and Tb^III ions (Scheme 1).[29, 30] This gap mismatch, which is already present for the visible emitting Ln^III ions, indicates that ZnS is inadequate to sensitize the near-infrared (NIR) emitting Ln^III ions (Ln = Yb or Nd). However, these ions are equally as interesting for imaging and sensing. We therefore decided to use CdS NPs as sensitizers of NIR emission, as their band gap is at lower energy (bulk CdS = 2.4 eV or 19,360 cm^{-1}). As shown in

Department of Chemistry, University of Nevada, Reno, Nevada 89557-216, U. S. A.,
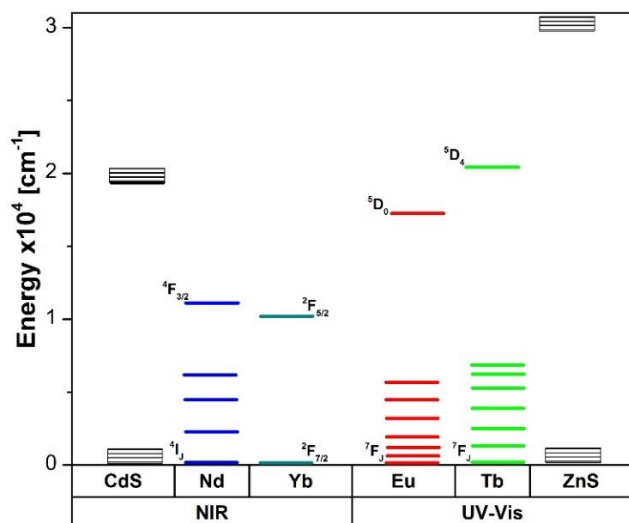 *Email - abd@unr.edu.*

Scheme 1, this system will be better matched to sensitize the NIR emitting ions.


Scheme 1. Energy level diagram of bulk CdS, ZnS and Ln[III] ions, showing that ZnS is more adequate to sensitize the visible emitting ions, while CdS is more adequate to sensitize the NIR-emitting ions.

The use of CdS NPs as sensitizers is particularly advantageous due to their high photostability, high photoluminescence quantum yield and the ease of tuning their emission wavelength by varying their size.[32] We adopted a simple hydrothermal method for synthesizing water-soluble, band gap tuneable, 3-MPA-capped CdS NPs (3-MPA-NPs).[33] The ability of the NPs to coordinate NIR emitting Ln[III] (Ln = Yb or Nd) ions (3-MPA-Ln-NPs) and sensitize the luminescence of the metal ions was investigated using infrared, NMR, UV-Vis absorption, excitation and emission spectroscopy. The structure and crystallinity of the 3-MPA-NPs and the 3-MPA-Ln-NPs systems were studied using transmission electron microscopy (TEM) and powder X-ray diffraction (XRD).

Results and discussion

CdS NPs were prepared using a one-pot non-injection hydrothermal method previously reported by Schneider and co-workers,[33] and shown in Scheme 2. The method allows for the average sizes of the NPs to be tuned by varying the heating time of the reaction. We chose reaction times of 30, 50 and 120 minutes. The particles were purified by centrifuging and washings with ethanol. Evidence for the removal of free 3-MPA and for the binding of the 3-MPA ligands to the NPs was provided by the absence of the S-H (2550 cm^{-1}) as well as the presence of the symmetric (1395 cm^{-1}) and asymmetric (1557 cm^{-1}) carboxylate stretching vibrations in the Fourier transform infrared (FT-IR) spectra of the 3-MPA-NPs (Figure 1).[29, 34-36]
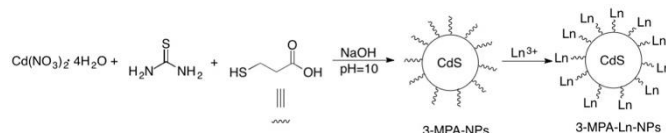
Scheme 2. Synthesis of 3-MPA-capped NPs (3-MPA-NPs) and of the Ln[III]-decorated 3-MPA-LnNPs.
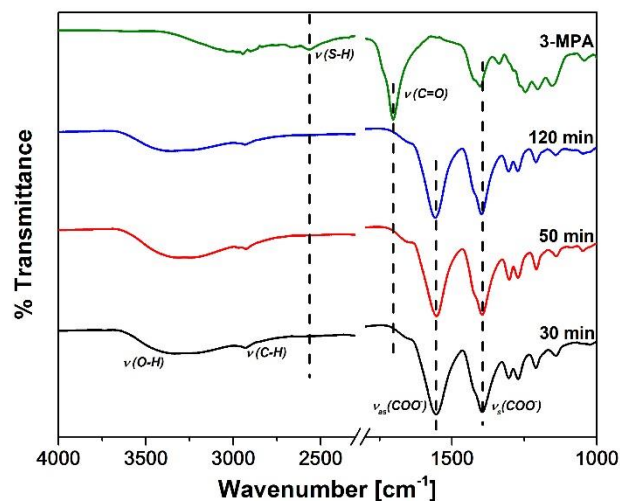

Figure 1. FT-IR spectra of the 3-MPA-NPs and 3-MPA with assignment of the vibrations of interest, ν(S-H), ν(C=O) and ν(COO[-]), marked with vertical dashed lines.

The binding of the capping 3-MPA ligand was further supported by ^{1}H NMR spectroscopy of solutions of the 3-MPA-NPs, as the proton resonances of 3-MPA are broadened following binding (Figures 2a-c, bottom red broad spectra) due to a lack of free rotation of the ligand once bound to the surface.[27, 37] Elemental composition analysis indicated the presence of significant amounts of C, S, O and Cd in the samples that are consistent with the targeted composition (Table S1).
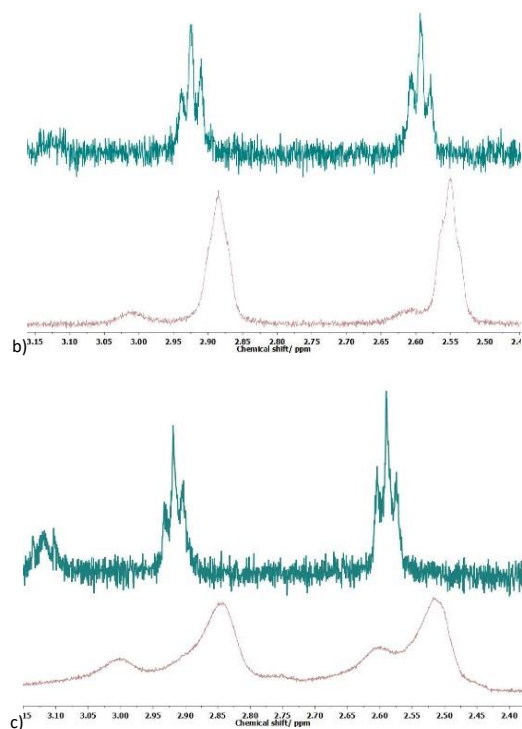
ARTICLE
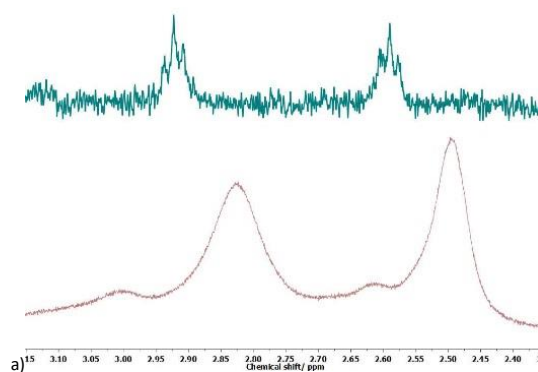
Figure 2. ¹H NMR spectra of the a) 30 min, b) 50 min and c) 120 min 3-MPA-NPs (bottom) and of their La^{III}-systems (top) in D$_2$O-DSS.

TEM images showed that the 3-MPA-NPs are monodisperse and crystalline with d-spacings of ~0.34 nm that correspond to a cubic structure (Figures 3a-c and insets). The average sizes were 3.5±0.2, 3.1±0.3 and 3.6±0.6 nm for the 30, 50 and 120 min 3-MPA-NPs, respectively (Table S2).

The cubic structure was corroborated by powder X-ray diffraction (XRD) analysis. The diffractograms show broad peaks at 2θ = 26° and 47° that correspond to the (111) and (220) planes of cubic CdS, respectively (Figure 4).[33] The broad diffraction peaks result from the small size of the NPs.[38]

The 30, 50 and 120 min 3-MPA-NPs showed UV-Vis absorption maxima at 358, 368 and 386 nm, respectively (Figure 5). This indicates that the photophysical properties are tuneable using varied heating times, as indicated by Schneider and co-workers.[33] The 30 min 3-MPA-NPs fluoresced green, while the 50 and 120 min ones fluoresced yellow (Figure 5 inset). The band gaps, estimated from the onset of the UV-Vis absorption

spectra, decreased with prolonged reaction times from 3.22 eV or 25,971 cm^{-1} for the 30 min NPs, to 3.12 eV or 25,164 cm^{-1} for the 50 min NPs and 3.01 eV or 24,277 cm^{-1} for the 120 min NPs. The tuneability of the band gaps was confirmed by the red-shifting of the excitation and emission spectra in water. The emission maxima are at 556, 574 and 592 nm, while the maxima of the excitation spectra were 356, 366 and 380 nm for the 30, 50 and 120 min NPs, respectively (Figure 6 top). A similar behaviour was observed for the solid-state samples (Figure 6 bottom). The fluorescence quantum yields were 2.0, 3.2 and 3.4% for the 30, 50 and 120 min NPs, respectively (Table 1). The fluorescence emission lifetimes of these 3-MPA-NPs in solution were fitted to second-order exponential decays, and are consistent with other reported lifetimes and the presence of core (long-lived) and surface (short-lived) states (Table 1 and Figures 7a and 7b).[39] The linear increase in emission quantum yields with increasing reaction time is consistent with results reported by Schneider and co-workers[33] (Table 3). However, the emission lifetimes of the 50 min 3-MPA-NPs were higher than the 30 min and 120 min ones in either H$_2$O, D$_2$O or in the solid-state (Table 1). Uosaki and co-workers[39] also observed this effect in CdS NPs, and attributed it to an increase in the interior trap states (crystal defects) with increasing NP size. In going from 30 min to 50 min, the increase in NP size leads to a decrease in the surface/volume ratio of the NPs, leading thus to a decrease in the surface states which act as recombination centers.[39]
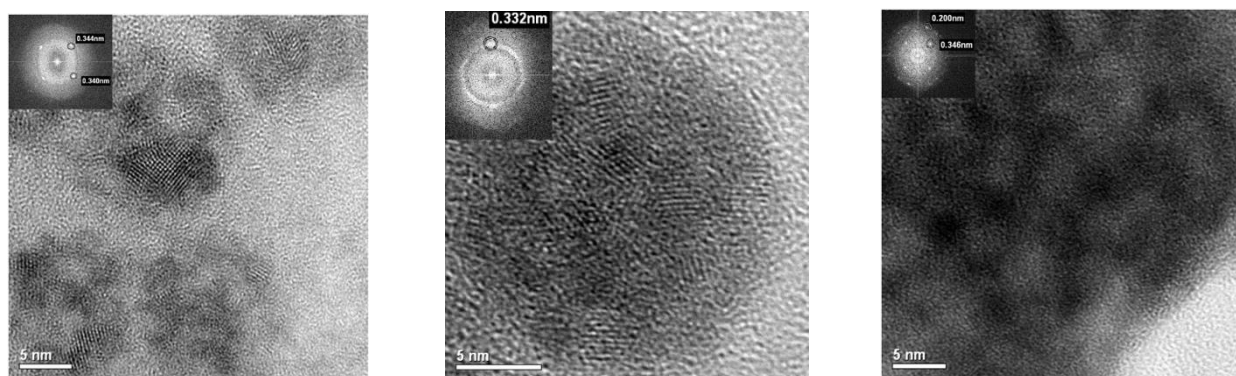

Figure 3. TEM images of the 30 (left) 50 (middle) and 120 min (right) 3-MPA-NPs. The insets show the lattice fringes and the d spacing.
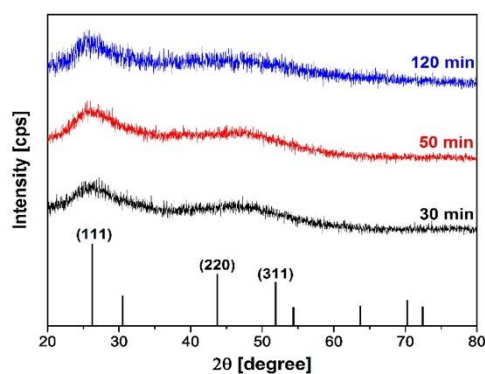
Figure 4. Powder XRD diffractograms of the 3-MPA-NPs. Bottom, CdS pattern, followed by systems grown for 30 (black), 50 (red) and 120 (blue) minutes.
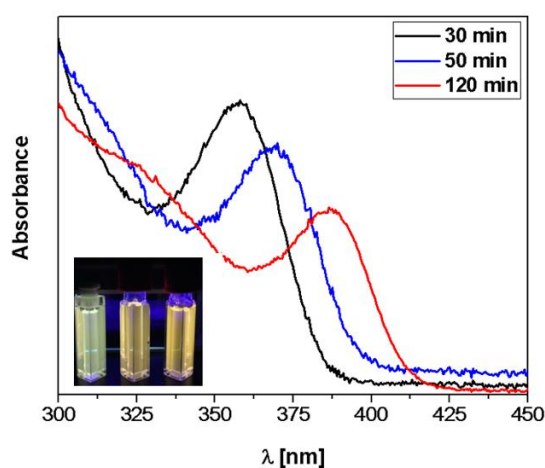

Figure 5. UV-Vis absorption spectra of the 3-MPA-NPs in water. The inset shows the fluorescence of the aqueous solutions of the 30 (left), 50 (middle) and 120 min (right) 3-MPA-NPs under UV-lamp irradiation.
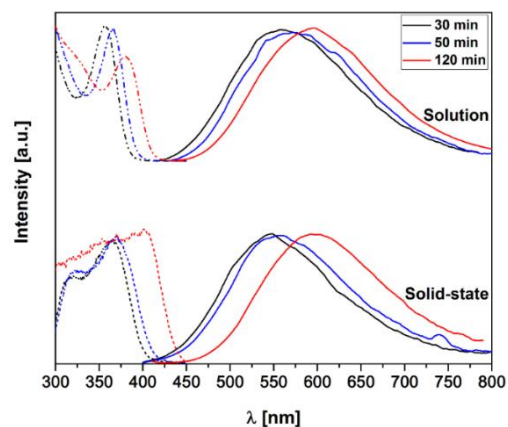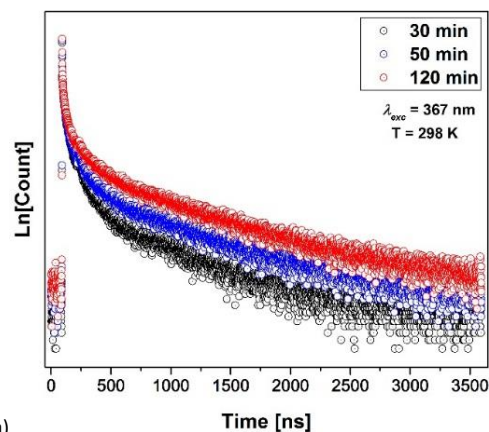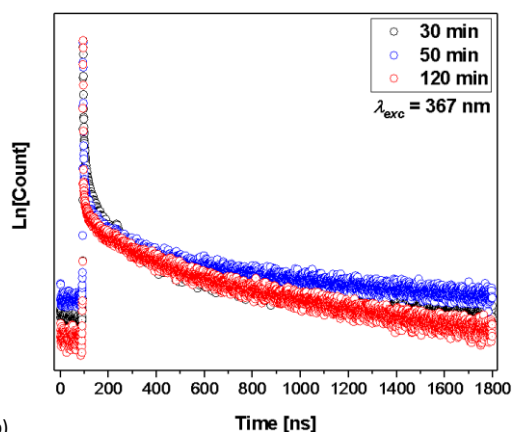

Figure 6. Excitation (dashed lines) and emission (solid lines) spectra of the 3-MPA- NPs in water (top) and in the solid-state (bottom).

Table 1. Fluorescence emission quantum yields, ϕ, and emission lifetimes, τ, of the 3-MPA-NPs obtained in H_2O and solid-state at 25.0±0.1 °C with λ_{exc} = 367 or 390 nm.

3-MPA-NPs	30 min	50 min	120 min
$\tau(H_2O)$ [ns]	45.3±2.3	49.7±4.2	33.8±2.0
	302.8±43.5	476.6±26.2	360.1±29.0
$\tau(D_2O)$ [ns]	34.9±7.5	39.3±6.1	35.8±2.5
	319.4±8.6	533.5±15.5	348.4±23.9
$\tau(solid)$ [ns]	20.1±0.2	22.0±0.4	21.7±1.1
	295.7±2.3	390.7±4.0	220.8±0.7
ϕ [%]	1.99±0.02	3.18±0.01	3.40±0.03

a)

b)

Figure 7. Emission decay curves of the 3-MPA-NPs in a) H_2O and b) solid-state.

Ln[III]-containing systems of the NPs (3-MPA-Ln-NPs) were prepared by stirring optimum amounts of the dried NP powders with the chloride salts of the Ln[III] (Yb or Nd) ions in deuterium oxide at room temperature overnight (Scheme 2). The optimum ratio of Ln[III] ions to NPs was determined by titrating Eu[III] ions with the NPs, which resulted in the observation of typical Eu[III] $^5D_0 \rightarrow ^7F_J$ *(J = 0-4)* transitions (Figure S1), and monitoring the emission intensity of the $^5D_0 \rightarrow ^7F_2$ transition of the Eu[III] at 615 nm (Figure S1a) as a function of added NPs. The intensity increased steadily to reach a maximum at 5.45 x 10^{-7} mol Eu[III] ions to 0.20 mg NPs; subsequent quenching of the Ln[III]-centred emission was attributed to aggregation effects.[30] The prepared Ln[III]-containing systems were purified by centrifuging to isolate the 3-MPA-Ln-NPs as powders.

Evidence for the coordination of the Ln[III] ions by the carboxylato groups of the capping ligands was confirmed by shifts in the asymmetric and symmetric vibrations of the carboxylato groups (Figures 8a-c and Table S3), from 1395 and 1554 cm^{-1} to 1405

and 1532 cm^{-1}, respectively, following coordination of the Ln^{III} ions (Figures 8a-c and Table S3).

The coordination of the Ln^{III} ions by the 3-MPA was further

crystallinity, cubic phase and average diameters of the NPs were unchanged following coordination of Ln^{III} ions to the surface 3-MPA ligands (Table S2, Figure 9 and insets).
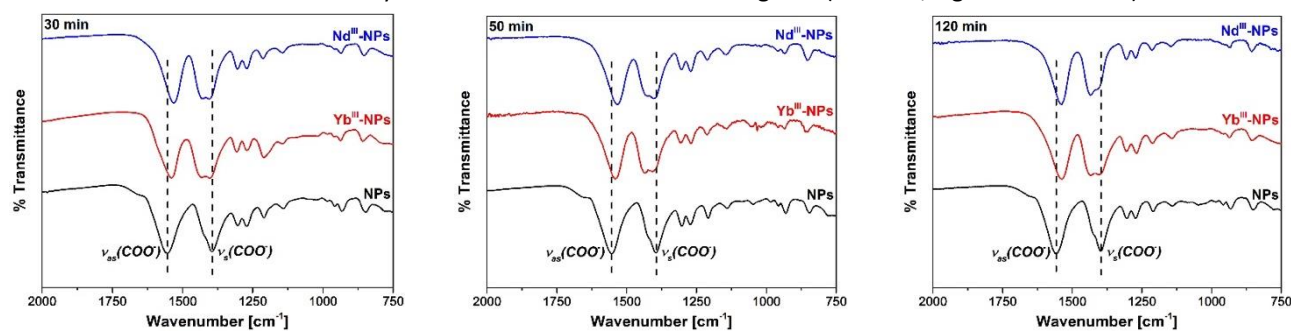

Figure 8. Infrared spectra of the 30 (left), 50 (middle) and 120 min (right) 3-MPA-NPs and their Yb^{III} and Nd^{III} systems, 3-MPA-Yb-NP and 3-MPA-Nd-NP. The carboxylato frequencies are marked with dashed vertical lines.
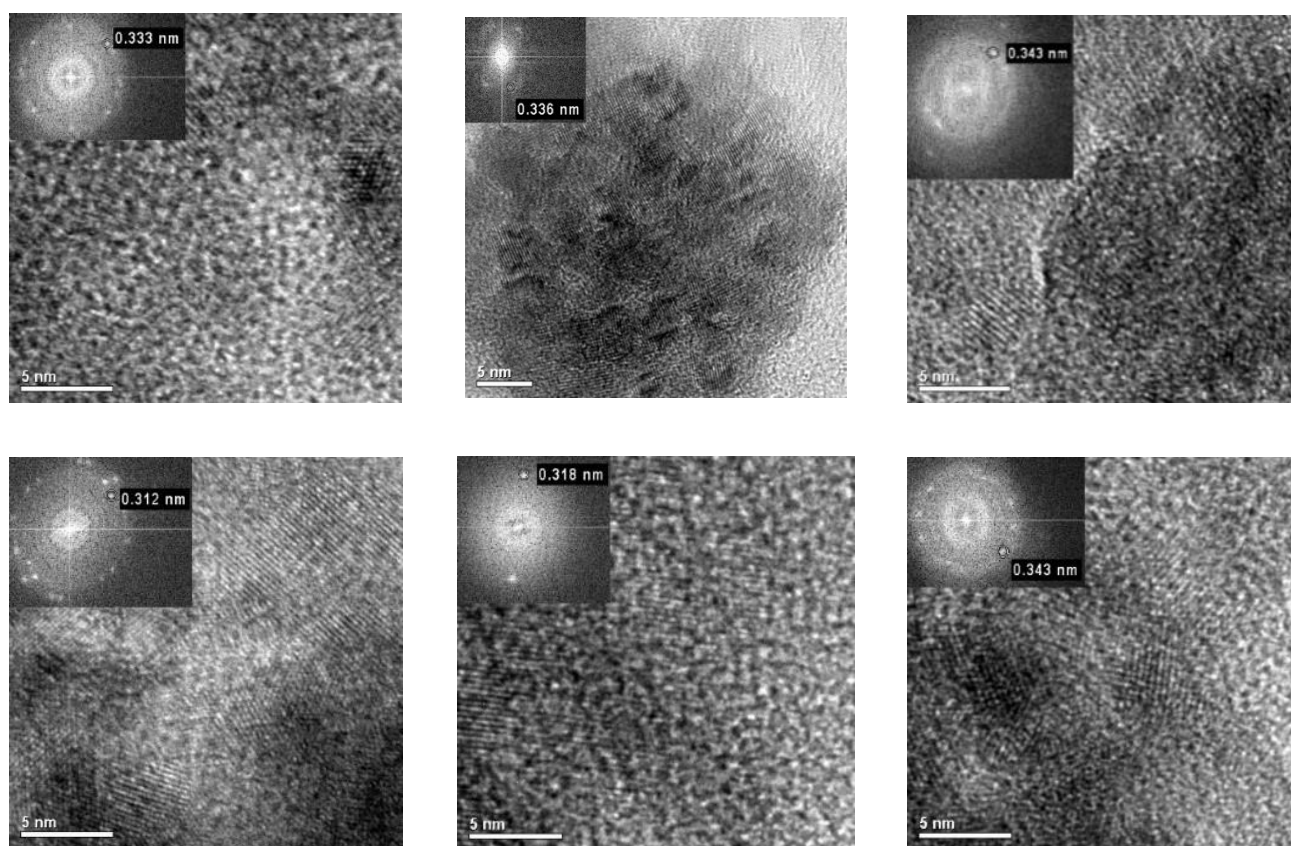

Figure 9. TEM images of the 30 (left), 50 (middle) and 120 min (right) NPs of the Nd^{III} (top) and Yb^{III} (bottom) 3-MPA-Ln-NPs. The insets show the lattice spacing.

confirmed by ^{1}H NMR spectroscopy of solutions of 3-MPA-Ln-NPs, with La^{III} as the diamagnetic metal ion. The proton resonance of the methylene group closer to the carboxylato at 2.82 ppm is shifted to 2.92 ppm following addition of the La^{III} salts (Figures 2a-c, top green spectra). The other methylene proton resonance was shifted from 2.50 ppm to 2.59 ppm after addition of the La^{III} salts (Figures 2a-c).

Addition of the Ln^{III} salts to the 3-MPA-NPs had no effect on the structure of the NPs, as the diffractograms show broad peaks that correspond to the (111) and (220) planes (Figures S2a-c), indicating that the NPs still have a cubic structure. Similarly, the

Excitation of the aqueous and solid-state 3-MPA-Ln-NP systems at the wavelength of NP absorption resulted in the typical $^4F_{3/2} \rightarrow ^4I_{11/2}$ (1058 nm) and $^2F_{5/2} \rightarrow ^2I_{7/2}$ (976 nm) transitions of Nd^{III} and Yb^{III}, respectively (Figure 10). While there is still significant residual NP fluorescence, the excitation spectra match the absorption spectra of the NPs, indicating that the Ln^{III}-centred emission is a result of energy transfer from the NPs to the Ln^{III} ions (Figures 5 and 10).

Table 2. Emission quantum efficiencies, ϕ, of the 3-MPA-Ln-NPs in D_2O at 25.0±0.1 °C obtained by exciting at 395 nm (Yb^{III}) or 380 nm (Nd^{III}) and with $Yb(tta)_3(H_2O)_2$ as emission standard.[40]

3-MPA-Ln-NP	30 min	50 min	120 min
Nd^{III} ϕ [%]	0.021±0.004	0.012±0.002	0.012±0.001
Yb^{III} ϕ [%]	0.010±0.005	0.010±0.005	0.010±0.002

To further validate that the energy is indeed transferred from the NPs to the coordinated Ln^{III} ions, aqueous solutions of the $LnCl_3$ salts and Ln^{III}-complexes (Ln = Yb or Nd) of 3-MPA, in absence of NPs, were excited at 380 nm. The excitation of the samples failed to yield typical Nd^{III}- or Yb^{III}-centred transitions in

NPs, in analogy to what was observed for the NPs without any Ln^{III} ions added (Tables 1 and 3). In comparison, the emission lifetimes of the 3-MPA-NPs were higher than the 3-MPA-Ln-NPs (Tables 1 and 3). This is a result of the energy transfer from the NPs to the Ln^{III} ions.

Table 3. Emission lifetimes, τ, of the NPs in the Yb^{III} and Nd^{III} systems 3-MPA-Ln-NPs in D_2O obtained at 25.0±0.1 °C at λ_{exc} = 367 or 390 nm.
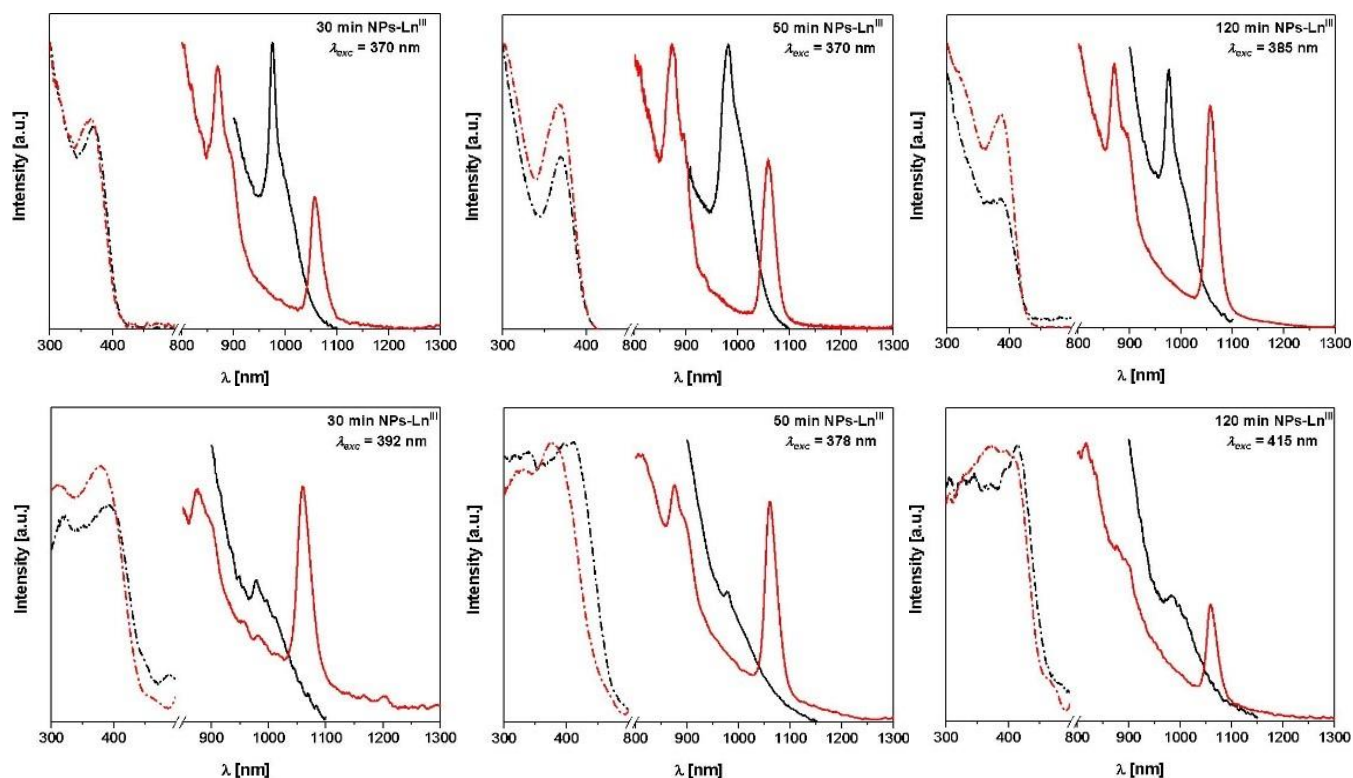

Figure 10. Excitation (dashed lines) and emission (solid lines) spectra of the 30 (left), 50 (middle) and 120 min (right) Ln^{III}-containing systems in D_2O (top) and solid-state (bottom).

the emission spectra (Figures S3a-b). Also, for these samples with only 3-MPA and Ln^{III} ions, monitoring the emission of Yb^{III} at 980 nm and Nd^{III} at 1064 nm resulted in the observation of f-f transitions of the Ln^{III} ions in their excitation spectra (Figures S3a-b). These observations confirm that the Nd^{III}- and Yb^{III}-centred emission is only sensitized in the presence of the NPs. The emission efficiencies were 0.02% and 0.01% for the Nd^{III} and Yb^{III} systems of the 30 min NPs, respectively (Table 3). In comparison, the emission efficiencies of the 50 min and 120 min systems were 0.01% for both Nd^{III} and Yb^{III} systems (Table 3). Comparison of the emission intensities of the solution and solid-state spectra showed weaker Ln^{III}-centred emission in the latter case, especially for the Yb^{III} systems, which was attributed to aggregation effects (Figures 10a-c).[41]

The luminescence emission lifetimes of the residual NP emission in the 3-MPA-Ln-NPs were also measured. The emission decay curves could be fitted to second-order exponentials, corresponding to core and surface states of the

τ [ns]	30 min-NPs	50 min-NPs	120 min-NPs
Nd^{III}	17.2±0.5	21.0±0.8	17.2±0.6
	247.7±24.2	399.7±17.5	166.9±1.2
Yb^{III}	32.5±2.7	38.7±1.9	23.6±0.9
	271.5±8.3	368.6±16.4	227.5±7.2

Conclusions

We successfully adopted a one-pot non-injection hydrothermal method to synthesize 3-MPA capped CdS NPs, 3-MPA-NPs. The NPs were water-soluble and the surface-bound 3-MPA chelated Ln^{III} ions via the carboxylato groups to yield new 3-MPA-Ln-NPs. These NPs sensitized NIR Ln^{III}-centred emission upon excitation at the wavelength of NP absorption with emission efficiencies of 0.02% and 0.01% for the 30 min Nd^{III} and Yb^{III} systems, respectively. The emission efficiencies for the Nd^{III} and Yb^{III} systems were 0.01% for both the 50 min and 120 min 3-MPA-Ln-NPs. The fluorescence lifetimes of the 3-MPA-NPs decreased

following addition of the NIR-emitting Ln^{III} ions, which indicates the transfer of energy from the NPs to the Ln^{III} ions. These systems are examples of new infrared luminescent materials with potential application in imaging.

Experimental

Millipore water (18.0 MΩ) was used for all syntheses and spectroscopy. The infrared spectra were recorded using a Nicolet 6700 FT-IR spectrometer in the range $600 - 4000$ cm^{-1} with 4 cm^{-1} resolution in ATR mode. The NMR spectra were acquired using Varian NMR instruments operating at 400 or 500 MHz. The UV-Vis absorption spectra were acquired on a PerkinElmer Lambda 35 spectrometer, whereas the excitation and emission spectra were acquired on a Horiba Nanolog fluorimeter equipped with a 450 W xenon (Ushio) lamp. Both excitation and emission spectra were corrected for instrumental response function. The emission lifetimes of the NPs were recorded in TCSPC mode using either a 367 or 394 nm peak wavelength NanoLED. Powder XRD data were acquired using a Bruker D2 Phaser equipped with a Cu radiation (Kα = 1.5418) source operating at 30 kV and 10 mA with 3.0 mm air-scatter filter. TEM and EDX analyses were done using a JEOL-2100F field emission transmission electron microscope, equipped with an Oxford energy dispersive spectrometer.

Synthesis of 3-MPA-NPs
54.0 mg (0.175 mmol) of cadmium nitrate tetrahydrate and 22.0 mg (0.289 mmol) of thiourea were dissolved in 14 mL of water, a 20 mL aqueous solution of 34.4 μL (0.395 mmol) of 3-MPA was added and the pH adjusted to 10 with 0.1 M NaOH. The solution was bubbled with nitrogen for 30 min before the mixture was transferred into a pressure vessel under nitrogen and sealed. The vessel was heated at 100°C for either 30, 50 or 120 min and allowed to cool to room temperature before the pressure vessel was opened. The NPs were precipitated with ethanol and the mixture was centrifuged for 10 min at 10^4 rpm to isolate the NPs. The NPs were washed twice with ethanol and centrifuged as before. The isolated NPs were dried under vacuum at room temperature.

Emission quantum yield measurements
The emission quantum yields were measured using a Horiba Jobin Yvon Nanolog integrating sphere coated with Spectralon which has a flat 95% reflectance in the range $250 - 2500$ nm. The emission quantum yields ϕ of the NPs in H$_2$O were determined using equation 1.

$$\phi = \frac{E_c - E_a}{L_a - L_c} \qquad \text{Eq. 1}$$

E and L denote the integrated luminescence and integrated excitation areas, respectively. The subscripts a and c denote the blank (sample holder with solvent) and sample, respectively.[42]

The quantum yield measurements of the Ln^{III}-containing NP systems were determined in D$_2$O by comparing against an air-saturated $Yb(tta)_3(H_2O)_2$ standard in toluene (ϕ = 0.12%).[40] The

systems were diluted to achieve an absorbance A$\leq$0.3 at 380 nm (Nd^{III} systems) or 395 nm (Yb^{III} systems) and both the samples as well as the standard were excited at the same wavelength to allow for reasonable emission signal detection and a linear relationship between the intensity of light absorbed and emitting species. The quantum yield, ϕ_x, of each system was determined using equation 2.

$$\phi_x = \phi_{ST} \times \frac{n_x^2 \, A_{ST} \, E_x}{n_{ST}^2 \, A_x \, E_{ST}} \qquad \text{Eq. 2}$$

n is the refractive index of the solvent, A is the absorbance at A$\leq$0.3 and E is the integrated area of the emission spectrum. Subscripts x and ST denote the sample and standard, respectively.[5]

Determination of the Ln^{III}/NP ratio
3-MPA-Ln^{III}-NP systems were prepared by mixing 50 μL of EuCl$_3$ [1.09 x 10^{-2} M] with 100 μL incremental aliquots of the NPs [0.24 mg/mL] and diluting each to 5.0 mL, followed by stirring at 300 rpm for 18 h at room temperature. Emission spectra of the aliquots were then acquired and the emission intensity of the $^5D_0\rightarrow^7F_2$ transition of Eu^{III} monitored as a function of added NPs. The optimum ratio determined from the titration experiment was 50 μL (5.45 x 10^{-6} mol) of Ln^{III} to 800 μL (0.19 mg) of NPs.

Synthesis of 3-MPA-Ln-NPs
These systems were prepared in an analogous manner to the solutions for the titration experiments, using the optimum ratio of Ln^{III} to 3-MPA-NPs.

Conflicts of interest

There are no conflicts to declare.

Acknowledgements

References

1. J.-C. G. Bünzli *Chem. Rev.*, 2010, **110**, 2729-2755.
2. S. Eliseeva and J.-C. G. Bünzli *Chem. Soc. Rev.*, 2010, **39**, 189-227.
3. J.-C. G. Bünzli and C. Piguet, *Chem. Soc. Rev.*, 2005, **34**, 1048-1077.
4. A. de Bettencourt-Dias, *Luminescence of lanthanide ions in coordination compounds and nanomaterials*, John Wiley & Sons, 2014.
5. A. de Bettencourt-Dias, *Curr. Org. Chem.*, 2007, **11**, 1460-1480.
6. D. Liu, Y.-N. Zhou, J. Zhao, Y. Xu, J. Shen and M. Wu, *J. Mater. Chem. C*, 2017, 11620-11630.
7. A. de Bettencourt-Dias and J. S. K. Rossini, *Inorg. Chem.*, 2016, **55**, 9954-9963.

8.   Z. Wu, M. D. Lee, T. J. Carruthers, M. Szabo, M. L. Dennis, J. D. Swarbrick, B. Graham and G. Otting, *Bioconjugate Chem.*, 2017, **28**, 1741-1748.

9.   A. de Bettencourt-Dias, P. S. Barber, S. Viswanathan, D. T. de Lill, A. Rollett, G. Ling and S. Altun, *Inorg. Chem.*, 2010, **49**, 8848-8861.

10.   P. Mukherjee, R. F. Sloan, C. M. Shade, D. H. Waldeck and S. Petoud, *J. Phys. Chem. C*, 2013, **117**, 14451-14460.

11.   D. Kim, N. Lee, Y. I. Park and T. Hyeon, *Bioconjugate Chem.*, 2017, **28**, 115–123.

12.   C. Meier, A. Gondorf, S. Lüttjohann, A. Lorke and H. Wiggers, *J. Appl. Phys.*, 2007, **101**, 103112.

13.   H. Doh, S. Hwang and S. Kim, *Chem. Mater.*, 2016, **28**, 8123–8127.

14.   B. A. Ashenfelter, A. Desireddy, S.-H. Yau, T. Goodson Iii and T. P. Bigioni, *J. Phys. Chem. C*, 2015, **119**, 20728–20734.

15.   J. Vela, B. S. Prall, P. Rastogi, D. J. Werder, J. L. Casson, D. J. Williams, V. I. Klimov and J. A. Hollingsworth, *J. Phys. Chem. C*, 2008, **112**, 20246-20250.

16.   M. E. Foley, R. W. Meulenberg, J. R. McBride and G. F. Strouse, *Chem. Mater.*, 2015, **27**, 8362-8374.

17.   W. Niu, S. Wu, S. Zhang and L. Li, *Chem. Commun.*, 2010, **46**, 3908-3910.

18.   F. Wang and X. Liu, *J. Am. Chem. Soc.*, 2008, **130**, 5642-5643.

19.   V. Buissette, D. Giaume, T. Gacoin and J.-P. Boilot, *J. Mater. Chem.*, 2006, **16**, 529-539.

20.   K. Riwotzki and M. Haase, *J. Phys. Chem. B*, 1998, **102**, 10129-10135.

21.   P. Saha Chowdhury and A. Patra, *Phys. Chem. Chem. Phys.*, 2006, **8**, 1329-1334.

22.   J. W. Stouwdam and F. C. J. M. van Veggel, *ChemPhysChem.*, 2004, **5**, 743–746.

23.   D. A. Chengelis, A. M. Yingling, P. D. Badger, C. M. Shade and S. Petoud, *J. Am. Chem. Soc.*, 2005, **127**, 16752-16753.

24.   G. A. Hebbink, J. W. Stouwdam, D. N. Reinhoudt and F. C. J. M. van Veggel, *Adv. Mater.*, 2002, **14**, 1147–1150.

25.   C. Sun, G. Pratx, C. M. Carpenter, H. Liu, Z. Cheng, S. S. Gambhir and L. Xing, *Adv. Mater.*, 2011, **23**, H195–H199.

26.   A. Escudero, C. Carrillo-Carrión, M. V. Zyuzin and W. J. Parak, *Top. Curr. Chem.*, 2016, **374**, 48.

27.   M. Irfanullah, D. K. Sharma, R. Chulliyil and A. Chowdhury, *Dalton Trans.*, 2015, **44**, 3082-3091.

28.   P. Agbo and R. J. Abergel, *Inorg. Chem.*, 2016, **55**, 9973–9980.

29.   R. A. Tigaa, G. J. Lucas and A. de Bettencourt-Dias, *Inorg. Chem.*, 2017, **56**, 3260-3268.

30.   J. K. Molloy, C. Lincheneau, M. M. Karimdjy, F. Agnese, L. Mattera, C. Gateau, P. Reiss, D. Imbert and M. Mazzanti, *Chem. Commun.*, 2016, **52**, 4577-4580.

31.   R. A. Tigaa, J. H. S. K. Monteiro, S. Silva-Hernandez and A. de Bettencourt-Dias, *J. Lumin.*, 2017, **192**, 1273-1277.

32.   M. Ethayaraja, C. Ravikumar, D. Muthukumaran, K. Dutta and R. Bandyopadhyaya, *J. Phys. Chem. C*, 2007, **111**, 3246-3252.

33.   A. Aboulaich, D. Billaud, M. Abyan, L. Balan, J.-J. Gaumet, G. Medjadhi, J. Ghanbaja and R. Schneider, *ACS Appl. Mater. Interfaces*, 2012, **4**, 2561-2569.

34.   M. Wang, W. Niu, X. Wu, L. Li, J. Yang, S. Shuang and C. Dong, *RSC Adv.*, 2014, **4**, 25183-25188.

35.   I. Hocaoglu, M. N. Cizmeciyan, R. Erdem, C. Ozen, A. Kurt, A. Sennaroglu and H. Y. Acar, *J. Mater. Chem.*, 2012, **22**, 14674-14681.

36.   S. T. Liu, T. Zhu, Y. C. Wang and Z. F. Liu, *Mol. Cryst. Liq. Cryst. Sci. Technol., Sect. A*, 1999, **337**, 245-248.

37.   A. M. Smith, L. E. Marbella, K. A. Johnston, M. J. Hartmann, S. E. Crawford, L. M. Kozycz, D. S. Seferos and J. E. Millstone, *Anal. Chem.*, 2015, **87**, 2771-2778.

38.   Y. Arao, Y. Hirooka, K. Tsuchiya and Y. Mori, *J. Phys. Chem. C*, 2008, **113**, 894-899.

39.   I. Yagi, K. Mikami, K. Ebina, M. Okamura and K. Uosaki, *J. Phys. Chem. B*, 2006, **110**, 14192-14197.

40.   M. P. Tsvirko, S. B. Meshkova, V. Y. Venchikov, Z. M. Topilova and D. V. Bol'shoi, *Opt. Spektrosk.*, 2001, **90**, 669-673.

41.   J. R. Lakowicz, *Principles of fluorescence spectroscopy*, Second edition. New York : Kluwer Academic/Plenum, 1999.

42.   J. C. de Mello, H. F. Wittmann and R. H. Friend, *Adv. Mater.*, 1997, **9**, 230–232.

TOC
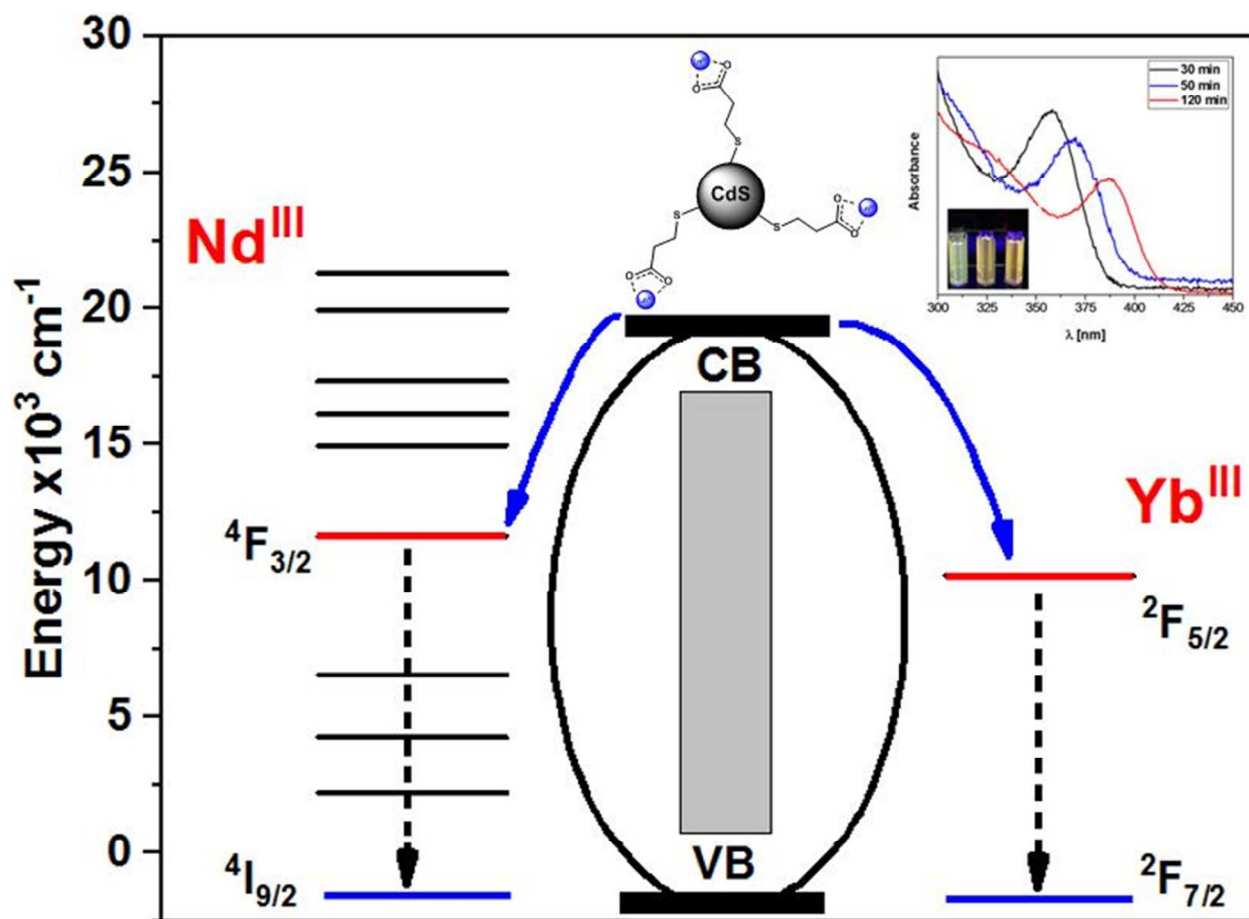
3-MPA capped CdS nanoparticles sensitize the NIR emission of Nd[III] and Yb[III].